

This is an Open Access document downloaded from ORCA, Cardiff University's institutional repository:<https://orca.cardiff.ac.uk/id/eprint/144002/>

This is the author's version of a work that was submitted to / accepted for publication.

Citation for final published version:

Li, Jiangxia, Pan, Shunqi , Chen, Yongping and Gan, Min 2021. The performance of the copulas in estimating the joint probability of extreme waves and surges along east coasts of the mainland China. *Ocean Engineering* 237 , 109581. [10.1016/j.oceaneng.2021.109581](https://doi.org/10.1016/j.oceaneng.2021.109581)

Publishers page: <http://dx.doi.org/10.1016/j.oceaneng.2021.109581>

Please note:

Changes made as a result of publishing processes such as copy-editing, formatting and page numbers may not be reflected in this version. For the definitive version of this publication, please refer to the published source. You are advised to consult the publisher's version if you wish to cite this paper.

This version is being made available in accordance with publisher policies. See <http://orca.cf.ac.uk/policies.html> for usage policies. Copyright and moral rights for publications made available in ORCA are retained by the copyright holders.



1 **The performance of the copulas in estimating the joint probability of extreme**
2 **waves and surges along east coasts of the mainland China**

3 Jiangxia Li^{a,b}, Shunqi Pan^c, Yongping Chen^{d,e,*}, Min Gan^e

4 a School of Hydraulic Engineering, Changsha University of Science and Technology, Changsha,
5 410114, China

6 b Key Laboratory of Water-Sediment Sciences and Water Disaster Prevention of Hunan Province,
7 Changsha, 410114, China

8 c Hydro-environmental Research Centre, School of Engineering, Cardiff University, Cardiff, CF24
9 3AA, United Kingdom

10 d State Key Laboratory of Hydrology-Water Resources and Hydraulic Engineering, Hohai
11 University, Nanjing, 210098, China

12 e College of Harbour, Coastal and Offshore Engineering, Hohai University, Nanjing, 210098, China

13 **Abstract**

14 In designing coastal and nearshore structures, the joint probability of the wave heights and storm
15 surges is essential in determining the possible highest total water level. The key elements to
16 accurately estimate the joint probability are the appropriate sampling of the extreme values and
17 selection of probability functions for the analysis. This study is to provide a full assessment of the
18 performance of the different methods employed in the joint probability analysis. The bivariate
19 extreme wave height and surge samples are analysed using 2 different probability distributions and
20 the performance of 4 copulas, namely: Gumbel–Hougaard copula, Clayton copula, Frank copula
21 and Galambos copula, is assessed. The possible highest total water levels for 100-year return period
22 along the coastline of the mainland China are estimated by the joint probability method with the
23 Gumbel–Hougaard copula. The results show that the wave heights and surges are highly correlated
24 in the areas of dense typhoon paths. The distributions of the possible highest total water levels show
25 a higher value in the southeast coast and lower value in the north. The results also indicate that at
26 the locations where the sea states are energetic, the joint probability approach can improve the
27 accuracy of design.

28 **Key words:** Coast of the mainland China; Joint probability; Copula; Extreme wave height; Extreme
29 surge level

30 **1. Introduction**

31 Designing the coastal and offshore structures requires the consideration of a broad range of ocean
32 factors due to complexity of the environment surrounding them. Amongst them, extreme waves and
33 storm surges are two main factors. Under severe meteorological conditions, such as those during
34 typhoons or cold storms, the extreme waves and storm surges can be closely correlated due to their
35 driving forces. Joint probability analysis commonly becomes essential in estimating the extreme
36 water levels to ensure the effective and sustainable designs of coastal engineering structures as
37 demonstrated in the studies of Serafin and Ruggiero (2014) and Wahl et al (2015).

38
39 In joint probability analysis, a wide range of probability distributions of simultaneous
40 environmental variables are obtained with the bivariate methods, as used by Ferreira and Guedes
41 Soares (2002), Galiatsatou and Prinos (2007). Furthermore, Bruun and Tawn (1998) compared the
42 properties of two extreme value methods: the univariate structure variable method and multivariate
43 joint probability method, and found that the latter provided more useful and accurate design
44 information when applied to several sites along Dutch coastlines. Based on a marginal distribution
45 function fitted to the water level and wave height and their dependence, Hawkes et al. (2002)
46 conducted a joint probability analysis, which was seen to perform better than the commonly used
47 structure variable approach and joint exceedance approach.

48
49 However, during the last few decades, the copula theory, which has been initially used in finance,
50 insurance and other economic sectors, has been widely adopted for joint probability analysis in the
51 fields of hydrology (Mikosch, 2006) and coastal engineering (Salvadori et al., 2015). A copula
52 function can connect different environmental variables without any hypothesis about their marginal
53 distributions, and provides a powerful tool for the joint analysis of multivariate data. Recent
54 examples of adopting the copula theory in hydrology fields include the study of extreme rainfalls
55 (Salvadori and De Michele, 2004; Zhang and Singh, 2007), flood frequency for rivers (Chen et al.,
56 2012; Sraj et al., 2015) and droughts (De Michele et al., 2013).

57
58 In coastal engineering applications, the copula theory has been found to be useful in providing

59 increased flexibility in modelling the joint probabilities of ocean hydrodynamic variables. As stated
60 in Coles et al (1999), quantifying dependence plays an importance role in the joint probability
61 analysis. In dealing with the dependence between two variables, Wist and Myrhaug (2004)
62 modelled two successive wave heights exceeding a certain threshold by a Gaussian copula and
63 compared the results with field measurements and laboratory data. De Waal and van Gelder (2005)
64 analysed the joint probability of extreme wave height and wave period using the Burr–Patero–
65 Logistic copula. Similar studies were also conducted by Montes–Iturrizaga and Heredia–Zavoni
66 (2015), as well as Vanem and Erik (2016). Wahl et al. (2010) carried out a study between two storm
67 surge parameters using the Gumbel–Hougaard (GH) copula. Chini and Stansby (2010) used an
68 integrated modelling system to investigate the joint probability of the extreme wave heights and
69 water levels at Walcott, on the eastern coast of UK for determining the changes in the overtopping
70 rates. Gruhn et al. (2012) used the Frank copula to estimate the joint probability of the water level
71 residuals and significant wave heights along the coast of the Baltic Sea. Wahl et al. (2012) applied
72 Archimedean copula functions in the German Bight to determine the exceedance probabilities of
73 storm surges and wind waves. Masina et al. (2015) used a copula-based approach to estimate the
74 joint probability of the water levels and waves at the Ravenna coast in Italy. The probability of
75 failure/inundation was estimated by the direct integration method, and the coastal flooding risks
76 were calculated. Galiatsatou and Prinos (2016) applied the copula method to investigate the changes
77 in the joint probabilities of extreme wave heights and corresponding storm surges with time in the
78 Aegean Sea. Ward et al. (2018) used the copula models to analyse the dependence between sea level
79 and river discharge as well as the probability of flooding events in global deltas and estuaries.
80 Bevacqua et al. (2019) discovered a higher probability of compound flooding from precipitation and
81 storm surge in Europe under climate change using a copula-based multivariate probability model.

82

83 For extreme events, Gudendorf and Segers (2010) proposed the extreme value copulas for extreme
84 multivariate analysis due to their capability of describing the upper tail dependence well. Mazas and
85 Hamm (2017) used an event-based approach for determining extreme joint probabilities of waves
86 and sea levels by focusing on the sampling of extreme events. In their study, three extreme value
87 copulas (GH copula, Galambos copula, Husler–Reiss copula) were compared, and their results
88 showed that different extreme value copulas would yield similar results, but the sampling methods

89 could cause a large difference in the joint probability results. The samples could be selected by
90 different ways. For example, in the sampling of extreme wave heights and surges, some researchers
91 sample the extreme wave heights (or surges) and the simultaneous surges (or wave heights) by the
92 block maxima method (Li and Song, 2006). Others consider the “impact” of the events and select
93 the samples according to a defined response function, i.e. total water levels, overtopping and run-up
94 (Gouldby et al., 2014; Serafin et al., 2014; Rueda et al., 2016). Also, the extreme pairs of samples
95 by defining the storm events using certain thresholds of variables are used (Li et al., 2014; Wahl et
96 al., 2016).

97
98 For multivariate cases, the dependence among a large range of extreme ocean elements like wave
99 height, water level, wave period, storm duration, etc. was assessed. Corbella and Stretch (2012,
100 2013) investigated the dependence between storm parameters: significant wave height, peak wave
101 period, duration, inter-arrival time, and water level, by applying a copula-based statistical model
102 under varying climatic conditions. Li et al. (2014) analysed the variates of extreme storm events
103 (wave height, wave period, sea level, wave direction, and storm duration) under deep-water wave
104 conditions, where the Monte Carlo method and four other methods to construct the dependency
105 structures based on the copula functions, physical relationship, and extreme value theory were
106 adopted. It was found that the Gaussian copula model was the most suitable wave climate
107 simulation method for the Dutch coast. Rueda et al. (2016) used the generalized extreme value
108 (GEV) distributions and Gaussian copula to model the dependence between multivariate extremes
109 related to coastal floods for different weather patterns. Lin-Ye et al. (2016) applied a hierarchical
110 Archimedean copula to characterize storm intensity based on the storm energy, unitary energy, peak
111 wave period, and duration on the Catalan coast. Montes–Iturrizaga and Heredia–Zavoni (2016)
112 developed a multivariate model for the joint distributions of environmental variables using vine
113 copulas, which was applied to build trivariate environmental contours of the wave height, period,
114 and wind velocity at the Gulf of Mexico. Zhang et al. (2018) modelled multivariate ocean data
115 using asymmetric copulas and compared the results with those obtained by traditional copulas.

116
117 The applications to the coastal waters of China are also seen rapidly emerging in recent years. Tao
118 et al. (2013) developed a criterion to classify the intensity grade of a storm surge by the joint return

119 period of the extreme water levels and wave heights in Qingdao. Yang and Zhang (2013) applied the
120 GH copula to analyse the joint probability of extreme winds and wave heights at the Bohai Bay.
121 Dong et al. (2015) used the Clayton copula to clarify the relations between the group height and
122 length of ocean waves based on laboratory data and field wave data near the coast of Zhejiang
123 province. Dong et al. (2017) studied the joint return probability of the wind speed and rainfall
124 intensity in a typhoon-affected sea area close to Shanghai using the Weibull distribution and GH
125 copula. More recently, Yin et al. (2018) estimated the extreme sea levels in the Yangtze estuary
126 using the quadrature joint probability optimal sampling method (JPM-OS) with consideration of the
127 typhoon field, wave height, and sea level in the studied region. Yang and Qian (2019) analysed the
128 joint probability of typhoon-induced surges and rainstorms at Shenzhen and derived trivariate joint
129 distributions and conditional distributions of these variables based on the copula method.

130

131 To estimate the desired design combination of wave height and surge accurately under extreme
132 conditions can be rather challenging. Many studies have outlined that a univariate frequency
133 analysis may not be capable of assessing the occurrence probability of extremes if the events are
134 characterized by interrelated random variables (Chebana and Ouarda, 2011; Masina et al., 2015).
135 According to Marcos et al. (2019), the return periods of extreme sea levels are underestimated in 30%
136 of the coasts around the world if dependence is neglected. In particular, along the coasts of China,
137 Li and Song (2006) analysed the correlations between the extreme wave heights and extreme water
138 levels in the coastal waters of Hong Kong using the Gumbel–logistic model. The result proved that
139 applying the commonly used empirical method to estimate the total water level (by directly adding
140 the univariate extreme values) may not be sufficiently accurate to derive the coastal design criteria.
141 On the other hand, because of the lack of long-term matched oceanic data, most of the previous
142 studies only focused on a limited area or specific observation station. Therefore, it is necessary to
143 carry out further research to clarify the relationships between extreme wave heights and storm
144 surges and devise a realistic and safe design in coastal and offshore engineering.

145

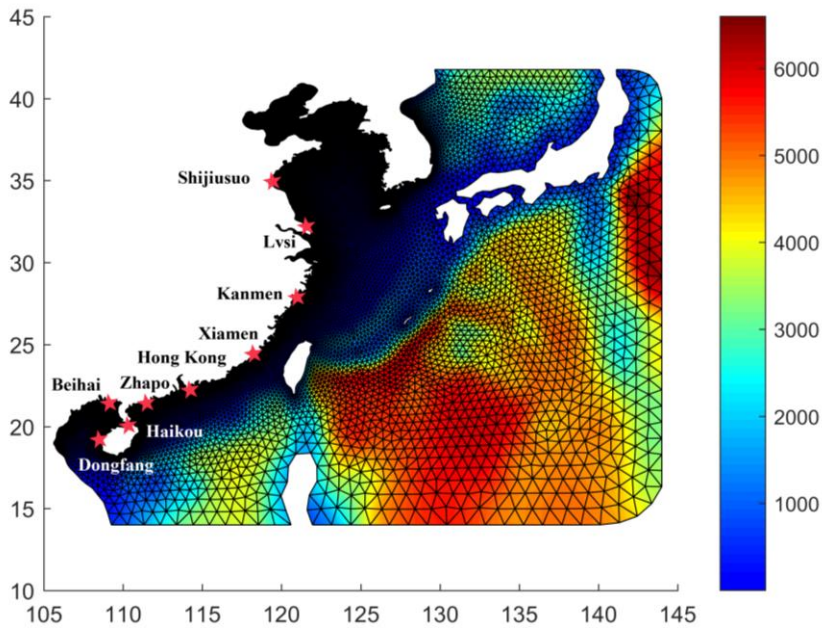
146 Built on the model results from the previous work of Chen et al. (2019), which used the GH copula
147 in analysing the joint probability of the wave height and surge along the coast of the mainland
148 China, this study is to fully examine the performance of four different types of copulas using the

149 existing model results from Chen et al. (2019) in estimating the joint probability. This study uses the
150 annual N-largest sampling method with a detailed analysis of the predominance of joint extreme
151 samples, in an attempt to effectively increase the available sample size compared to previous
152 studies. Then a comprehensive analysis of the dependence between wave height and surge is
153 conducted on the extreme samples obtained. The established joint probability model is subsequently
154 applied to 87 selected locations representing the entire mainland China coast, to estimate the
155 extreme combined water levels (CWLs) for flood risk assessment.

156

157 **2. Study area and data**

158 In this study, the model results of the significant wave heights (H_s) and surge levels (S) over a
159 35-year (1979–2013) period as detailed in Li et al. (2018) are used. For the sake of completeness,
160 the model setup and applications are briefly presented here. The computational domain covered an
161 area from 105 °E to 140 °E and from 15° N to 41 °N, as shown in Fig. 1. A coupled wave
162 (FVCOM-SWAVE) and hydrodynamic (FVCOM) model (Qi et al., 2009), which was well
163 calibrated and validated in the nearshore and offshore area by Li et al. (2018), was used. The model
164 used an unstructured mesh with a spatial resolution of 1 degree at the open boundaries and finer
165 than 0.1 degree in the coastal areas. Along the open boundaries, the model was driven by the tide
166 conditions obtained from TPXO database. The modified ECMWF re-analysis wind data with a
167 parametric typhoon model in order to account for the effects of 862 typhoons during the simulation
168 period was used as the sea surface forcing. Hourly wave height and surge data from the model at
169 nine nearshore locations which are identical to those in Chen et al. (2019), as shown in Fig. 1, are
170 extracted from the model results and used for the joint probability analysis in this study. The
171 selection of those nearshore locations is mainly due to the availability of field measurements for
172 validating the hydrodynamic model.



173

174 *Fig. 1 Model area/mesh and the locations of the nine nearshore stations along the mainland China coast for*
 175 *applications (colour represents the water depth, m)*

176

177 3. Methodology

178 3.1 Sampling method

179 For extreme analysis, sampling of the extreme values from the time series is a key step. When the
 180 data length is sufficiently long, the annual maximum (AM) method is commonly used to select the
 181 joint extreme samples to ensure the independence of extreme samples (Sraj et al., 2015; Yang and
 182 Zhang, 2013). However, according to the studies of Bernardara et al. (2014) and Mazas and Hamm
 183 (2017), for effective bivariate analysis, the sample size should be normally more than 300.
 184 Therefore, in most cases, the AM method may only generate a small sample size of extreme events,
 185 insufficient to effectively capture the information of the dependence between the variables. To
 186 overcome this, the peak over threshold (POT) method can be the effective one for selecting
 187 multivariate samples (Li et al., 2014; Mazas et al, 2014). Compared to the block maxima approach,
 188 POT method is advantageous when selected peaks result from different storm events. However, the
 189 POT-based joint sampling methods can present with the major difficulty in determining the values
 190 of the thresholds, particularly in the cases of highly variable hydrodynamic conditions temporally
 191 and spatially over a large study area such as this study.

192

193 Based on the block maximum sampling method for univariate analysis (Galiatsatou, 2011), in this
 194 study, an annual N-largest (ANL) joint extreme sampling method is proposed. This method selects
 195 the top N samples in each year such that it can capture more information than the AM method.
 196 Unlike the POT methods, the number of samples selected per year can be pre-determined in the
 197 ANL method, so that the extreme conditions can be fairly represented over the study area. In
 198 addition, to ensure the independence of the extreme events selected, a standard storm length
 199 covering both sides of each peak is considered. The standard storm length generally ranges from 24
 200 to 72 hours in coastal storm analysis, following several previous studies (Basco and Walker, 2010;
 201 Martzikos et al., 2021; Marcos et al., 2019). It is set to be 48 hours in this study after conducting a
 202 sensitivity test suggested by Tawn (1988): provided the storm length is approximately correct the
 203 estimates of quantiles should not change too much by making small changes to this length. The
 204 simultaneous S is selected within the standard storm length along with the N-largest Hs to account
 205 for the possible time lag between extreme Hs and S. The number of samples per year (N) can be set
 206 accordingly to meet the required sampling size. Thus, in this study, by considering data length
 207 available over the 35-year period and the required sample size for joint probability analysis
 208 suggested by Mazas et al. (2014), N = 10 is used.

209 3.2 Univariate probabilistic distributions

210 Before establishing the dependence between wave height (Hs) and surge level (S), a frequency
 211 analysis would be required for each variable to define its marginal distribution. The two
 212 probabilistic distributions as shown in Table 1 are tested in this study for searching the best fit of the
 213 samples:

214

215 *Table 1 The cumulative distribution function (CDF) of two probabilistic distributions*

Distribution	CDF
Pearson-III (P3)	$F_p(x) = \frac{[\frac{2}{\bar{x}C_v C_s}]^{C_s^2}}{\Gamma(\frac{4}{C_s^2})} \int_{a_0}^x (x - \bar{x} + \frac{2C_v}{C_s} \bar{x})^{\frac{4}{C_s^2}-1} \cdot \exp(-\frac{2}{\bar{x}C_v C_s} (x - \bar{x} + \frac{2C_v}{C_s} \bar{x})) dx$

where, Γ is the gamma function; \bar{x} is the mean value of the samples;

C_v and C_s are the coefficients of variation and skewness.

$$F_{gev}(x) = \exp\left(-\left(1 + k \frac{x - \mu}{\sigma}\right)^{-1/k}\right)$$

Generalized Extreme
Value (GEV)

where, μ , σ and k are the location, scale and shape parameters respectively.

216

217 3.3 Copulas

218 According to the theory of Sklar (1959), there exists a copula, C , that can connect the marginal
219 distributions, $u_1 = F_X(x)$ and $u_2 = F_Y(y)$, to form the CDF (Genest and Favre, 2003) expressed
220 as:

$$221 \quad F(x, y) = C(F_X(x), F_Y(y)) \quad (1)$$

222 The commonly used copula families include Gaussian copula, t-copula, extreme value copula
223 (EV-copula) and Archimedean copula. Among them, the Archimedean copula family has been
224 frequently applied to the hydrologic fields. Meanwhile, Gudendorf and Segers (2010) suggested that
225 EV-copula could also well describe the upper tail dependence for an extreme multivariate analysis.
226 Thus, in this study, three commonly used copulas under the Archimedean family: Gumbel-
227 Hougaard (GH) copula, Frank copula, and Clayton copula, together with an EV-copula, Galambos
228 copula, are examined. The EV-copula is a type of copula which not only satisfies all the definitions
229 and properties of copulas, but also meets the max-stable property for fixed integer n , i.e.

$$230 \quad \lim_{n \rightarrow \infty} C_F(u_1^{1/n}, \dots, u_d^{1/n})^n = C(u_1, \dots, u_d), \quad (u_1, \dots, u_d) \in [0, 1]^d \quad (2)$$

231 In fact, GH copula fits the properties of both Archimedean copula and EV-copula groups.

232

233 The generator function, CDF and probability density function (PDF) of these copulas are listed in
234 Table 2, where u_1 and u_2 are the marginal distributions and θ is the parameter of copula which
235 describes the dependencies. The Galambos copula which belongs to EV-copulas does not have a
236 generator function.

237 *Table 2 The generator function, CDF and PDF of four copulas*

Copula	Function	Functions
--------	----------	-----------

names	names	
Gumbel– Hougaard	generator	$\varphi(t) = (-\ln t)^\theta$
	function	
copula	CDF	$C(u_1, u_2, \theta) = e^{-[(-\ln u_1)^\theta + (-\ln u_2)^\theta]^{1/\theta}}$
	PDF	$c(u_1, u_2, \theta) = \frac{\{-1 + \theta + [(-\ln u_1)^\theta + (-\ln u_2)^\theta]^{1/\theta}\}}{u_1 u_2 e^{[(-\ln u_1)^\theta + (-\ln u_2)^\theta]^{1/\theta}}} \times (-\ln u_1)^{-1+\theta} \times (-\ln u_2)^{-1+\theta} [(-\ln u_1)^\theta + (-\ln u_2)^\theta]^{-2+1/\theta}$
Frank copula	generator	$\varphi(t) = -\ln \frac{e^{-\theta t} - 1}{e^{-\theta} - 1}$
	function	
	CDF	$C(u_1, u_2, \theta) = -\frac{1}{\theta} \ln \left[1 + \frac{(e^{-\theta u_1} - 1)(e^{-\theta u_2} - 1)}{e^{-\theta} - 1} \right]$
	PDF	$c(u_1, u_2, \theta) = \frac{\theta \cdot e^{\theta(1+u_1+u_2)} (1 + e^\theta)}{(e^\theta - e^{\theta+u_1} + e^{\theta u_1 + \theta u_2} - e^{\theta+u_2})^2}$
Clayton	generator	$\varphi(t) = \frac{1}{\theta} (t^{-\theta} - 1)$
	function	
copula	CDF	$C(u_1, u_2, \theta) = (u_1^{-\theta} + u_2^{-\theta} - 1)^{-1/\theta}$
	PDF	$c(u_1, u_2, \theta) = (1 + \theta)(u_1 u_2)^{-\theta-1} (u_1^{-\theta} + u_2^{-\theta} - 1)^{-2-1/\theta}$
Galambos	CDF	$C(u_1, u_2, \theta) = u_1 \times u_2 \times \exp\{((-\ln u_1)^{-\theta} + (-\ln u_2)^{-\theta})^{-\frac{1}{\theta}}\}$
	PDF	$c(u_1, u_2, \theta) = e^{[(-\ln u_1)^{-\theta} + (-\ln u_2)^{-\theta}]^{-1/\theta}} \times \{1 + (-\ln u_1)^{-\theta-1} \times (-\ln u_2)^{-\theta-1} \times [(-\ln u_1)^{-\theta} + (-\ln u_2)^{-\theta}]^{-2/\theta-2}\} \times [1 + (1 + \theta)[(-\ln u_1)^{-\theta} + (-\ln u_2)^{-\theta}]^{1/\theta}] - [(-\ln u_1)^{-\theta} + (-\ln u_2)^{-\theta}]^{-1/\theta-1} \times [(-\ln u_1)^{-\theta-1} + (-\ln u_2)^{-\theta-1}]$

238

239 3.4 Dependence

240 Several methods are available to determine the dependence structure between two random variables
241 X and Y. They are commonly used to calculate the correlation coefficients, for example, Pearson's r
242 correlation coefficient, Spearman's ρ coefficient, or Kendall's τ coefficient. In this study, Kendall's τ
243 coefficient is chosen to quantify the dependence between the Hs and S samples. It describes the
244 dependence between the samples by ranking the variables with the following expression:

$$\tau = \frac{(\text{number of concordant pairs}) - (\text{number of discordant pairs})}{n(n-1)/2} \quad (3)$$

where n is the total number of pairs. Any pair of observations, (x_i, y_i) and (x_j, y_j) , where $i \neq j$, is reckoned to be concordant if the ranks for both the elements agree, i.e., both $x_i < x_j$ and $y_i < y_j$ holds or both $x_i > x_j$ and $y_i > y_j$ holds, and otherwise is regarded as the discordant pair. Therefore, $\tau = 0$ indicates the perfectly independent cases and $\tau = 1$ indicates perfectly dependent cases.

Generally, in the extreme analysis, the dependency is determined for the extreme values. However, the correlation coefficients for the extreme values can be less capable of fully capturing the asymptotic dependency (Mazas et al., 2014). Thus, in this study, the chi-plots are used as graphical tools to assess the dependence between the extreme Hs and S. It supplements an ordinary scatterplot of the data by providing a graph that has characteristic patterns depending on whether the variates are independent, with some degree of monotone relationship or more complex dependence structure. Two variables (Λ_i, X_i) as suggested by Fisher and Switzer (1985, 2001) are used in the scatterplots as:

$$\Lambda_i = 4S_i \max \left\{ \left(F_i - \frac{1}{2} \right)^2, \left(G_i - \frac{1}{2} \right)^2 \right\} \quad (4)$$

$$X_i = (H_i - F_i G_i) / \{ F_i (1 - F_i) G_i (1 - G_i) \}^{\frac{1}{2}} \quad (5)$$

where,

$$S_i = \text{sign} \left\{ \left(F_i - \frac{1}{2} \right) \left(G_i - \frac{1}{2} \right) \right\} \quad (6)$$

$$F_i = \sum_{j \neq i} I(x_j \leq x_i) / (n-1) \quad (7)$$

$$G_i = \sum_{j \neq i} I(y_j \leq y_i) / (n-1) \quad (8)$$

$$H_i = \sum_{j \neq i} I(x_j \leq x_i, y_j \leq y_i) / (n-1) \quad (9)$$

and I is the indicator function.

268

269 The relationships between Kendall's coefficient τ and the correlation index, θ , for copulas
 270 introduced in Section 3.3 are listed in Table 3.

271

272 *Table 3 Relationships between Kendall's coefficient τ and parameter θ for different copulas*

Copula	Relationship
Gumbel–Hougaard copula	$\tau = 1 - 1/\theta$
Clayton copula	$\tau = \theta / (\theta + 2)$
Frank copula	$\tau = 1 + \frac{4}{\theta} \left[\frac{1}{\theta} \int_0^\theta \frac{t}{e^t - 1} dt - 1 \right]$
Galambos copula	$\tau = \frac{\theta + 1}{\theta} \int_0^1 \left(\frac{1}{s^{1/\theta}} + \frac{1}{(1-s)^{1/\theta}} - 1 \right)^{-1} ds$

273 **3.5 Return period**

274 In joint probability analysis, the bivariate return period can be defined. The OR return period (T_o)
 275 indicates that at least one of the variable exceeds a certain value, and the AND return period (T_a)
 276 indicates that both the variables exceed a certain value. They can be calculated using the following
 277 expressions:

278
$$T_o(x, y) = \frac{1}{1 - F(x, y)} \quad (10)$$

279 and

280
$$T_a(x, y) = \frac{1}{1 + F(x, y) - F_X(x) - F_Y(y)} \quad (11)$$

281 where $F_X(x)$ and $F_Y(y)$ are the marginal distributions and $F(x, y)$ is calculated by Eq. (1) by
 282 combining the CDF of the copula and corresponding marginal distributions.

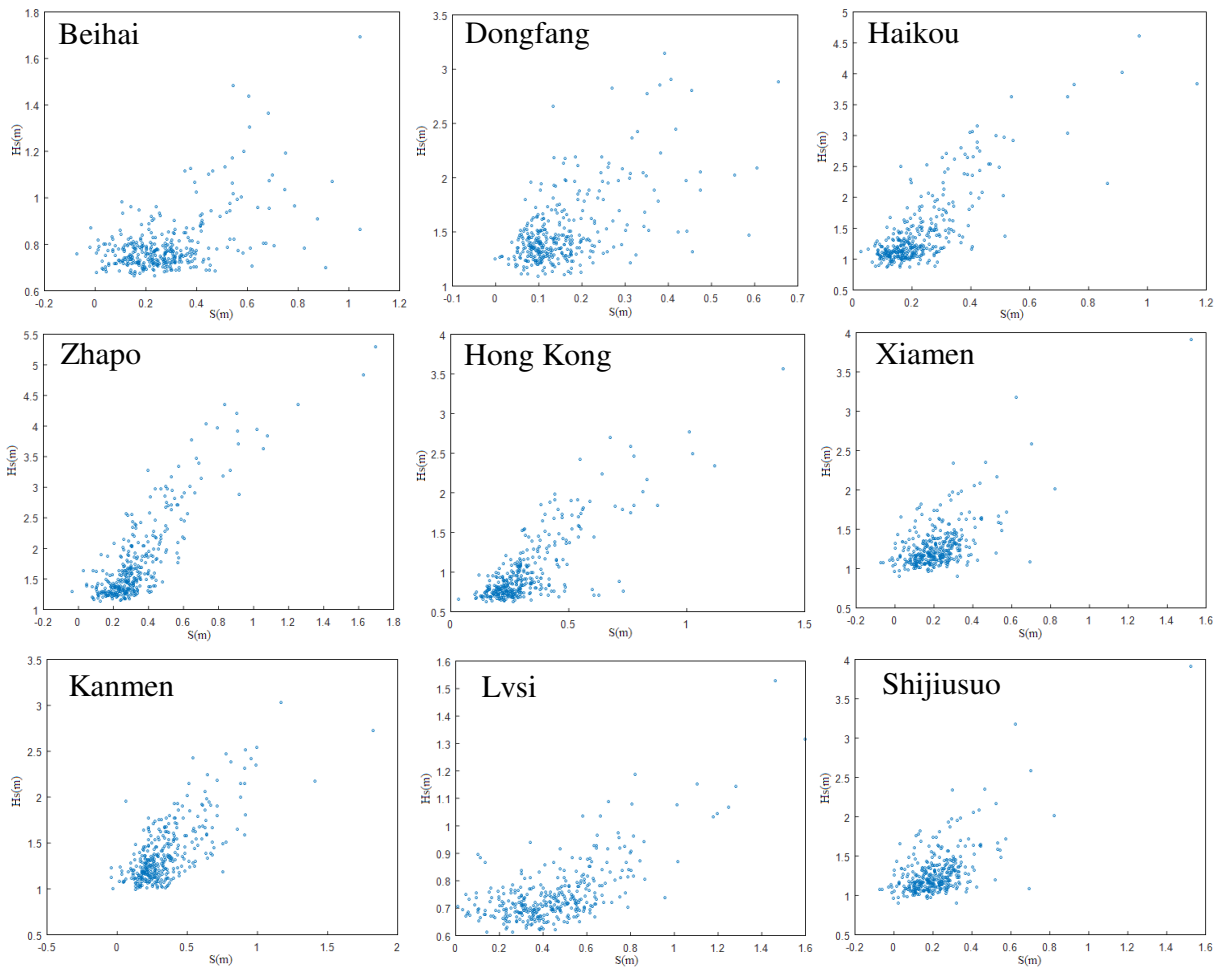
283

284 **4. Results**

285 **4.1 Dependence of extreme samples**

286 For the joint probability analysis, it is necessary first to examine the dependency between the
 287 extreme Hs and S. As an example, the extreme wave height (Hs) and surge (S) sampled at nine

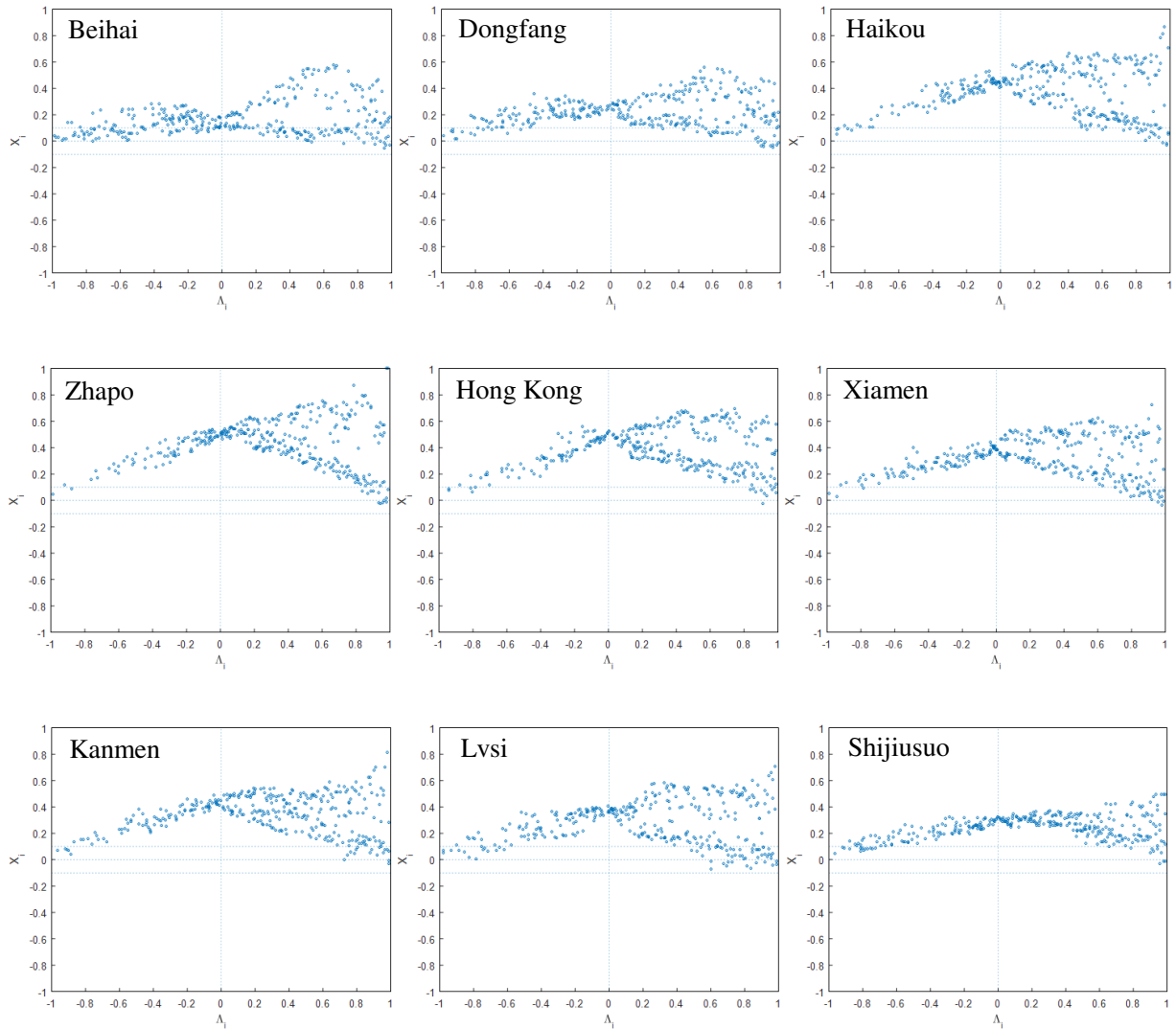
288 nearshore stations are shown in Fig. 2. It indicates that those two variables are partly related as the
 289 data points present a clear linear relation at all stations, but with a high degree of scattering.
 290 Relatively stronger dependencies between the extreme Hs and S are found at Haikou, Zhapo, Hong
 291 Kong, Xiamen and Kanmen stations because the scatters show a more obvious linear trend, but at
 292 other stations, such dependency appears relatively weaker. It is also noticed that the stations with
 293 stronger dependencies are located in the coastal areas facing the open sea and are easily affected by
 294 typhoon events. Stations Beihai and Dongfang are to some extent sheltered by the land. Stations
 295 Lvsi and Shijiusuo are located in the mid-north coast where fewer typhoon events occur. This result
 296 indicates that the dependencies between the extreme Hs and S at certain locations can be influenced
 297 by typhoon events.



298
 299 *Fig. 2 Scatterplot of the N-Largest joint samples*
 300

301 The chi-plots for all nine stations are shown in Fig. 3. In the chi-plot, Λ_i measures the distance of a
 302 pair of variables from their medians: a positive (negative) value implies that both variables are on
 303 the same (opposite) side of their respective medians and a value close to 1 (0) implies they are

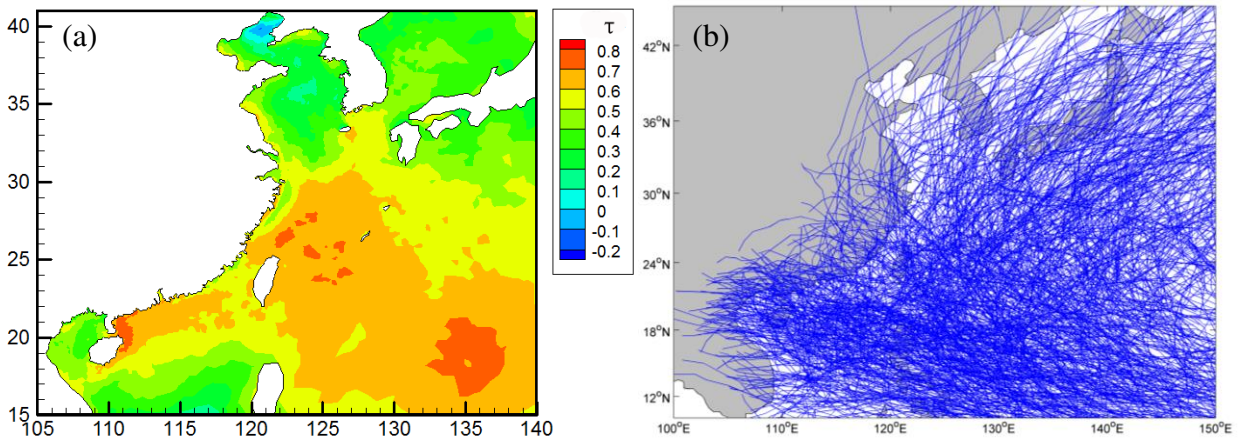
304 larger or smaller relative to (close to) their respective medians, and X_i measures the dependence: a
305 positive (negative) value describes a positive (negative) dependence, while a value close to zero
306 suggests independence (Mazas et al., 2014). From Fig. 3, it can be seen that there is a clear positive
307 dependence between the extreme Hs and S at all the stations. However, for the events where Λ_i is
308 negative, there is only one population at all stations, whilst for positive Λ_i , two different
309 populations are observed, namely, the upper and lower “lobes” as suggested by Fisher and Switzer
310 (2001). The upper “lobe” corresponds to pairs where both the Hs and S are larger than their median,
311 exhibiting a relatively strong dependence. This is because higher Hs and S are generally caused by
312 the same extreme atmospheric event. In contrast, the lower “lobe” corresponds to a pair where both
313 the Hs and S are smaller than their medians, exhibiting weak dependence. At most stations, there
314 are two distinct upper and lower lobes, which indicates the bimodal dependence of wave height and
315 surge due to relatively large events (such as typhoons) or weaker events. In other words, this
316 bimodal dependence could be caused by two extreme situations: typhoon related extremes and
317 non-typhoon related extremes. At the Shijiusuo station, however, the boundaries of the two “lobes”
318 are obscure, which may be attributed to the low frequency of typhoon events at this location.



319
 320 *Fig. 3 Chi-plots of the N-Largest joint samples*

321

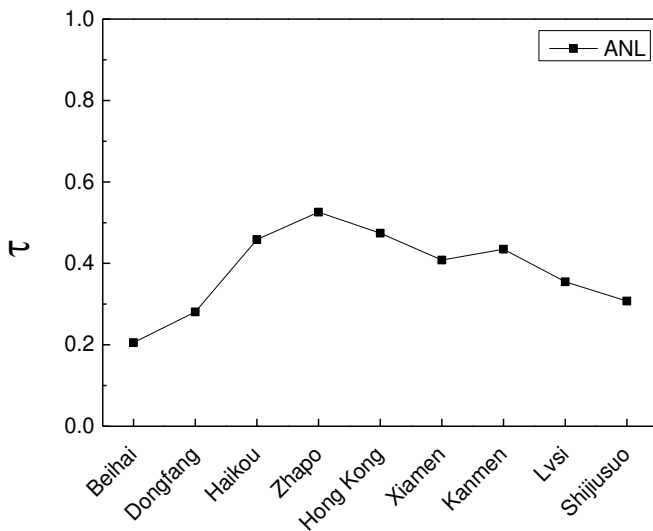
322 Furthermore, the distribution of Kendall's coefficient τ over the computational domain is also
 323 calculated, as shown in Fig. 4a. The results clearly show that the coefficients in the southeast area of
 324 the computational domain are remarkably larger than those at other locations, which coincides well
 325 with the areas along the paths of frequent typhoons during the 35-year (1979–2013) period (Fig. 4b).
 326 Specifically, the dependence between the extreme Hs and S increases in the areas where the sea
 327 states are more energetic, which was also reported in Hawkes et al. (2002). It is found that this
 328 character could not be fully revealed with the AM sampling method as used in Chen et al. (2019),
 329 which also serves as an indication of the improvement when the ANL sampling method is used.



330
 331 *Fig. 4 Distribution of (a) Kendall's coefficient τ and (b) the typhoon tracks from 1979 to 2013 in the study area*
 332

333 More specifically, the Kendall's coefficient τ at the nine nearshore locations is shown in Fig. 5. The
 334 results indicate that at Beihai, Dongfang, Lvsi, and Shijiusuo stations, values of τ are generally
 335 smaller compared to other stations, just below 0.35, suggesting relatively weak dependence between
 336 the extreme Hs and S at these stations. At other stations, particularly Zhapo and Hong Kong, the
 337 dependence between the extreme Hs and S is strong. According to Fig. 4 and Fig. 5, it seems that
 338 the stations in the areas frequently affected by typhoons tend to have large τ coefficients, as
 339 expected since typhoon events can be a significant cause for the extreme Hs and S.

340



341
 342 *Fig. 5 Kendall's coefficient τ between Hs and S at the nine nearshore stations*
 343

344 4.2 Marginal distributions

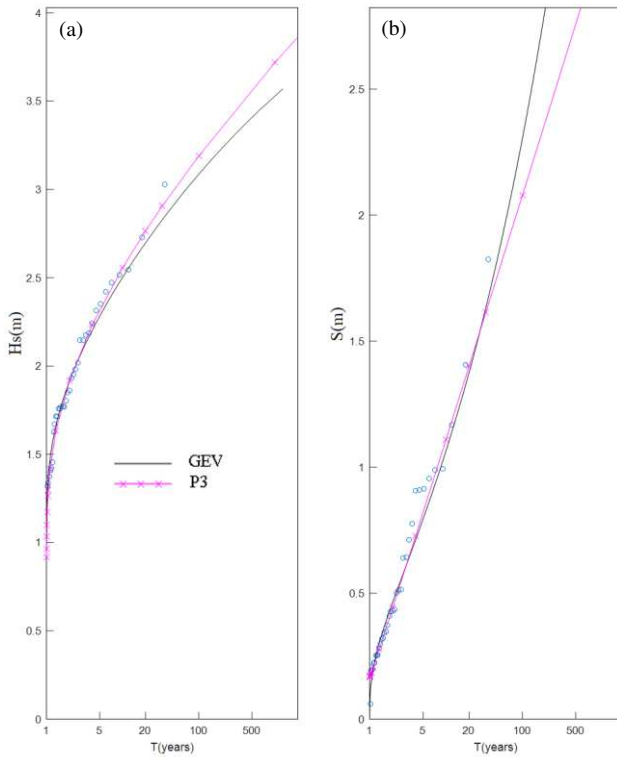
345 An advantage of applying the copula theory to bivariate or multivariate probability analysis is that
 346 copulas allow different types of marginal distributions to be used for different variables. To examine

347 the performance and fitness of copulas, in this study both Hs and S in the joint extreme samples at
 348 the nine nearshore locations are fitted with two univariate distributions as introduced previously.
 349 Since the study area is observed to be wave-predominated (discussed further in Section 6), extreme
 350 Hs data is sampled by the ANL method, and extreme S data is sampled based on the sampled Hs.
 351 By subsampling the N-largest data to annual maxima, two probability distributions introduced in
 352 Section 3.2 are used to fit the samples. The parameters in GEV are estimated by the maximum
 353 likelihood estimation method. In Fig. 6, the fittings of the Hs and S in the joint extreme samples
 354 with different distributions at the Kanmen station are plotted. Fig. 6 (a) shows that the P3
 355 distribution fits better the extreme Hs samples at Kanmen than GEV distribution, whereas in Fig. 6
 356 (b) the GEV distribution can comparatively better fit the extreme S samples.

357
 358 To quantify the fitting results, Pearson's coefficient r (Pearson, 1895) between the samples (dot in
 359 Fig. 6) and theoretical values (line in Fig. 6) are calculated at Kanmen station and listed in Table 4.
 360 The Pearson's coefficient r could be calculated by,

$$361 \quad r = \frac{\sum_{i=1}^n (X_i - \bar{X})(Y_i - \bar{Y})}{\sqrt{\sum_{i=1}^n (X_i - \bar{X})^2} \sqrt{\sum_{i=1}^n (Y_i - \bar{Y})^2}}. \quad (12)$$

362 where, X_i and Y_i are the sample values and the theoretical values; \bar{X} and \bar{Y} are the averaged
 363 values of X_i and Y_i . The largest correlation coefficients coincide with the best fit distribution
 364 chosen by Fig. 6.



365
366 *Fig. 6 Fitting of the samples with different distributions at Kanmen station: (a) wave height; (b) surge level*

367
368 *Table 4 Correlation coefficients between the samples and different distributions at Kanmen station (the best fit*
369 *distributions are indicated in bold)*

	GEV	P3
Wave height	0.9876	0.9877
Surge level	0.9921	0.9833

370
371 By combining the results in Fig. 6 and Table 4, the best fit distributions for the nine nearshore
372 stations are summarized in Table 5. It can be seen that GEV distributions fit the extreme Hs samples
373 better than P3 at 6 out of 9 stations, and the GEV distribution fits the extreme S samples better at all
374 stations in the study area. Although not shown here, the 95% confidence intervals of the selected
375 marginal are also examined to ensure a proper fit. It is reasonable to see that the confidence
376 intervals increase from the lower tail to the upper tail. Therefore, the distributions of the Hs and S
377 are determined by the selected probability distributions in this study.

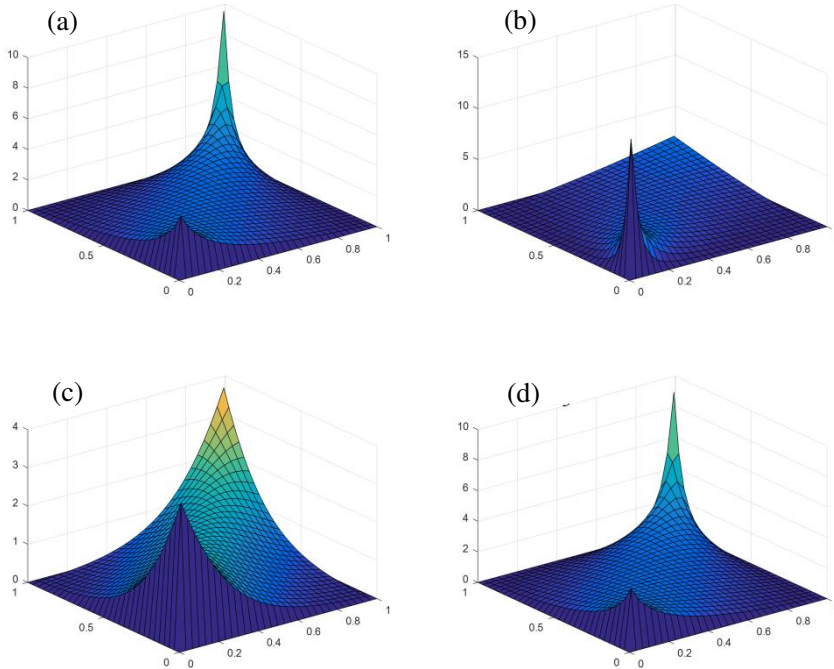
378
379 *Table 5 Chosen distributions for the Hs and S in the joint samples at the nine nearshore stations*

Station	Beihai	Dongfang	Haikou	Zhapo	Hong Kong	Xiamen	Kanmen	Lvsi	Shijiusuo
Hs	GEV	GEV	GEV	P3	P3	GEV	P3	GEV	GEV

380

381 4.3 Selection of copulas

382 To determine the best fit copulas for the data sets in this study with the chosen marginal
 383 distributions of the extreme Hs and S as described previously, it is essential to examine the
 384 characteristics of each copula. Fig. 7 shows the probability density distributions of the GH copula,
 385 Clayton copula, Frank copula, and Galambos copula. It is clear that both GH and Galambos copulas
 386 have a pronounced upper tail density, suggesting that they are capable of describing the dependence
 387 in the upper tail of the distribution, i.e. upper tail dependence. However, the density distribution of
 388 the Clayton copula has a thick lower tail density, suggesting that it can better describe the
 389 dependence in the lower tail of the distribution, i.e. lower tail dependence. The Frank copula has a
 390 symmetric tail, i.e. no tail dependence, which can only be suitable for the symmetrical distributed
 391 samples.



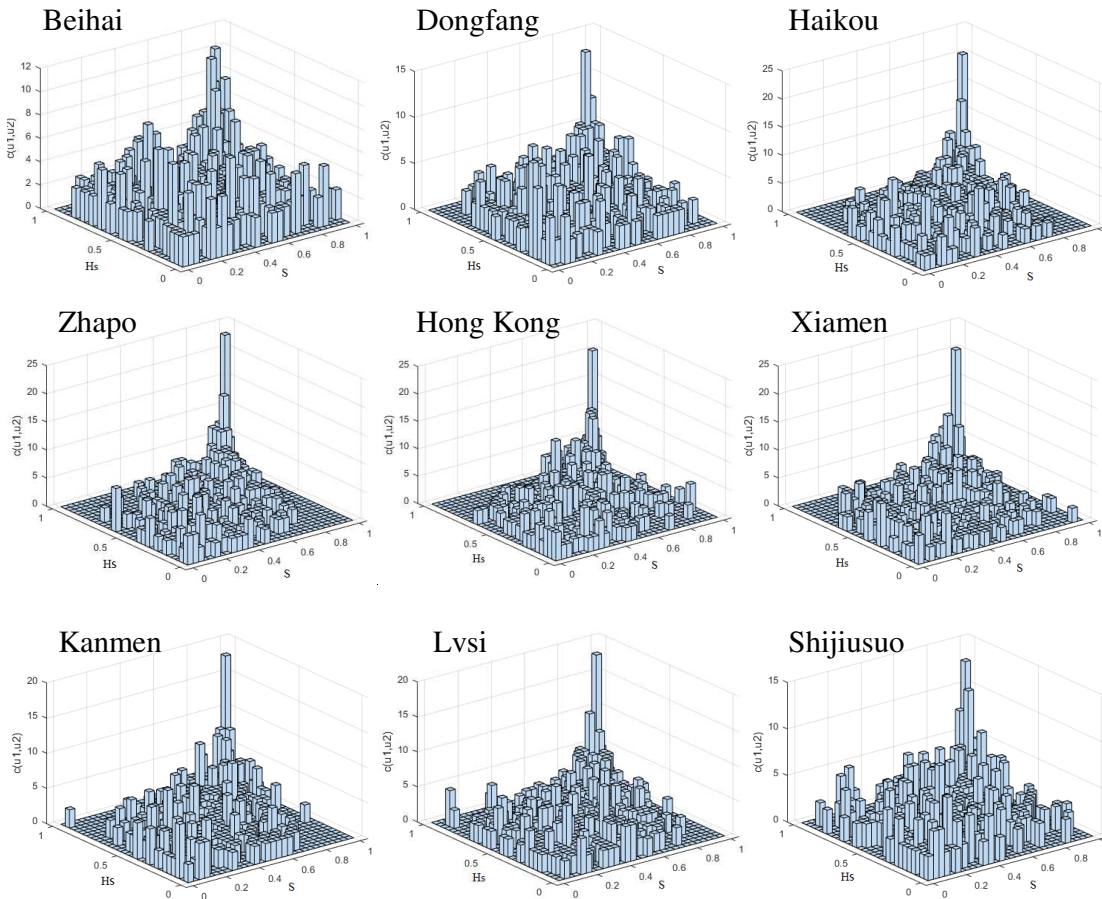
392

393 *Fig. 7 Probability density distributions of (a) GH copula, (b) Clayton copula, (c) Frank copula, and (d) Galambos*
 394 *copula*

395

396 To achieve the best match of the characteristics of the copulas shown in Fig. 7 with the samples in

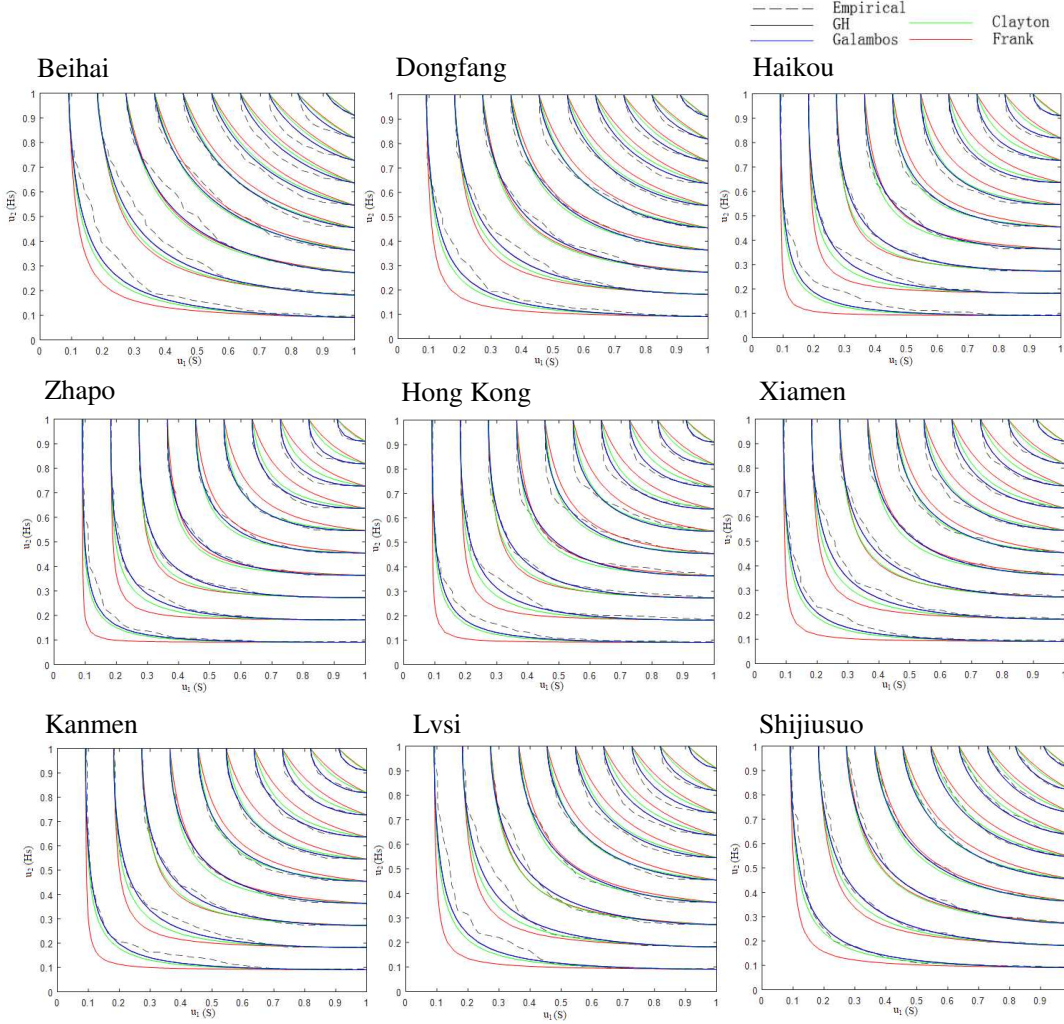
397 this study, the extreme samples at all nine stations are examined with the binary frequency
 398 histograms of the H_s and S . As shown in Fig. 8, at all stations, a thick upper tail density can be
 399 observed, although the frequency distributions are slightly different at different stations. In general,
 400 there is a clear suggestion that the GH copula and Galambos copula can be chosen in the probability
 401 analysis as they match well with all density distributions at those stations.
 402



403
 404 *Fig. 8 Binary frequency histograms of H_s and S in the joint samples*
 405

406 However, for the completeness of analysis, all four copulas are also used to fit the joint extreme
 407 samples using Kendall's coefficient as introduced in Section 3.5. Fig. 9 shows their joint cumulative
 408 probabilities in comparison with those of the empirical copula at all nine stations. As the probability
 409 of the empirical copula is directly calculated based on the samples, any copula in the test that has
 410 the best fit with the empirical copula will be regarded as the optimal copula for the samples. It can
 411 be seen from the comparisons that the contours of four copulas provide a very similar fit in the
 412 mid-range of probabilities. However, Clayton and Frank copula perform poorly with tendency of
 413 underestimating the probability in the upper tail region while overestimate the probability in the

414 lower tail region. This is related to the density distribution of those tested copulas. The results
 415 clearly show a general trend of good match of the GH and Galambos copulas with the empirical
 416 copula, better than the other two copulas, while Frank copula has the worst fit.



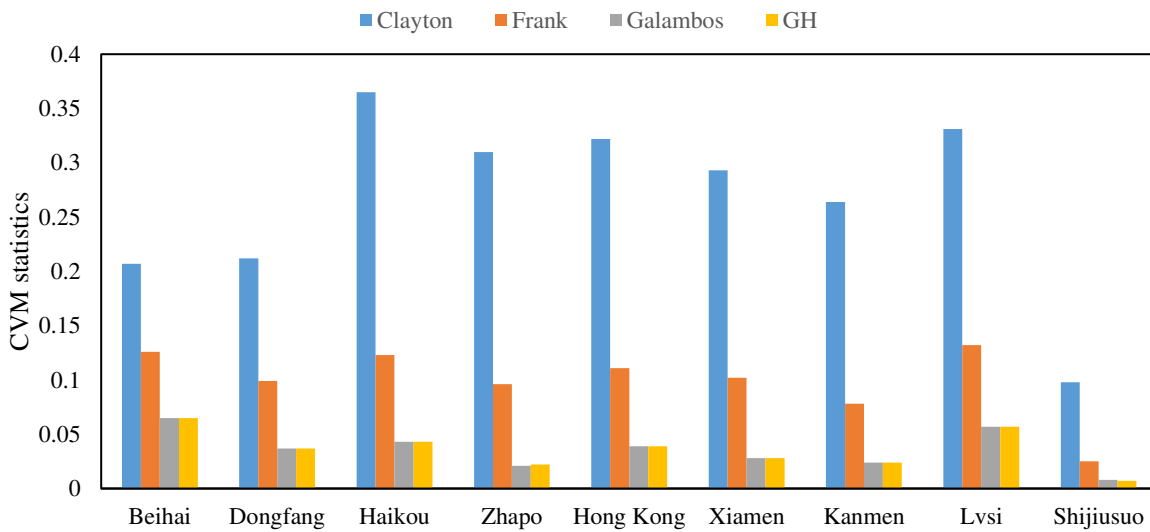
417
 418 *Fig. 9 Comparison of joint probability of four copulas with that of empirical copula*
 419

420 In addition, the Cramér-von Mises (CVM) test is carried out to compare the performance of the four
 421 copulas with that of the empirical copula quantitatively, using the following equation (Mazas and
 422 Hamm, 2017; Genest and Rivest, 1993):

$$423 \quad S_n = \sum_{i=1}^N [C_n(U_i, V_i) - C_\theta(U_i, V_i)]^2, \quad (13)$$

424 where, N is the sample size, (U_i, V_i) is the sample of the normalized ranks, C_n is the copula in
 425 test, and C_θ is the empirical copula. The CVM statistics at all stations are shown in Fig. 10. It is
 426 clear that CVM values for the Galambos and GH copulas are the lowest amongst all 4 copulas,
 427 while GH copula preforms slightly better than Galambos copula. The results again confirm the

428 outcomes of the probability density analysis of these copulas as shown in Fig. 7 and Fig. 8.

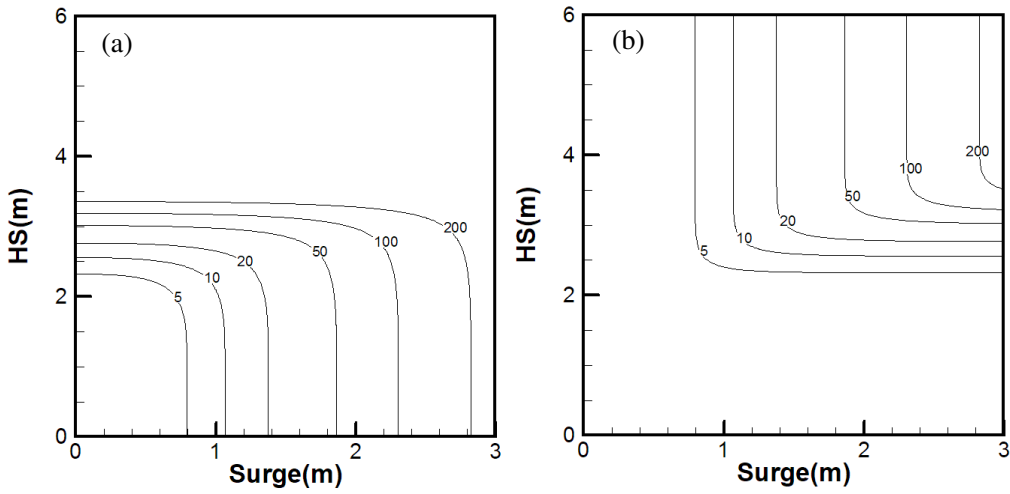


429
430 *Fig. 10 CVM statistics at the nine nearshore stations*

431
432 From the results presented in Fig. 10, it can be concluded that both GH and Galambos copulas,
433 which have the lowest CVM values amongst all, are deemed to be the optimal ones for studying the
434 joint probability of the extreme Hs and S along the east coast of the mainland China. It also
435 highlights the necessity of using an EV-copula to conduct the joint probability analysis of extreme
436 values. Considering that the GH copula has a simpler function than the Galambos copula, therefore
437 it is decided that the GH copula is adopted in this study.

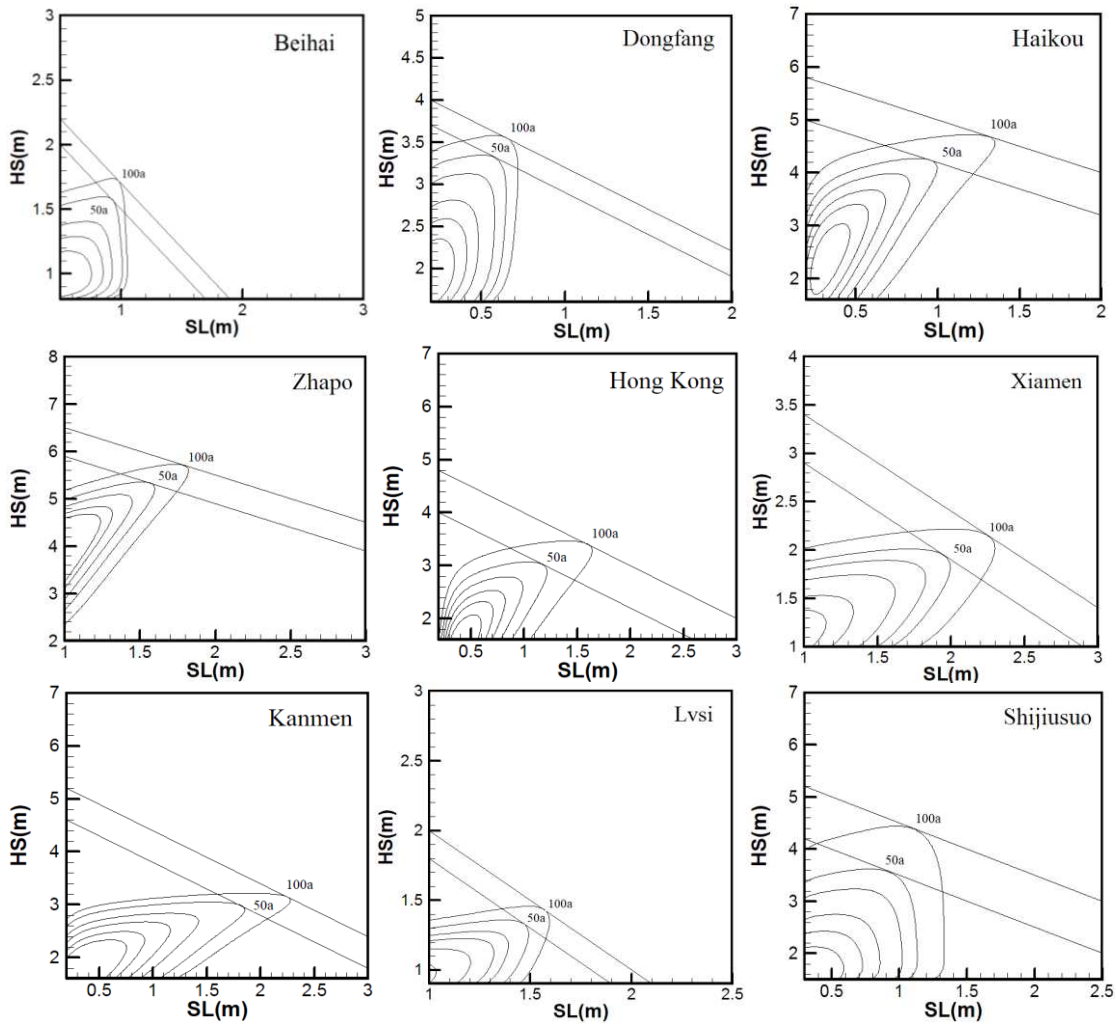
438 4.4 Joint probability

439 For the joint probability, both AND and OR return periods are assessed at all station. As an example,
440 the isolines of the joint events with both return periods at the Kanmen station are shown in Fig. 11.
441 In general, for the same joint event, the AND return period is found to be larger than the OR return
442 period. Specifically, when calculating the joint probability of the variables, the selection of the
443 different types of return period should be according to the aim of the study. In the following
444 analysis in this study, the AND return period is applied. Concurrently, according to a previous study
445 (Chen et al., 2019), the shapes of the isolines are diverse at different locations because the joint
446 probability is location-specific, particularly in the nearshore areas. Because the distributions of the
447 joint events at different locations are discussed in detail in a previous study (Chen et al., 2019), the
448 isolines of the joint events at other stations are not provided here.



449
 450 *Fig. 11 Isolines of (a) the AND return period and (b) the OR return period at the Kanmen station*
 451

452 From Fig. 11, it can be seen that different combinations of the Hs and S can have the same return
 453 period along an isoline when calculating the joint events by using a cumulative probability. Thus, to
 454 search for the most probable joint event for a certain return period, the joint probability density is
 455 the best function to be used. The combined water level (CWL) which is the sum of the Hs and S is
 456 analysed in this study for engineering application. To determine the most probable CWL, the joint
 457 probability density is calculated to obtain the failure probability by integration over the failure
 458 region (Masina et al., 2015; Chen et al., 2019). Along the isoline of the failure probability, the point
 459 corresponding to the highest probability density is the most probable extreme event, which is the
 460 tangential point between the isoline of the failure probability (indicated by straight lines in Fig. 12)
 461 and a particular isoline of the probability density (indicated by curves in Fig. 12). Then the extreme
 462 CWL is calculated by adding the Hs and S of the most probable extreme event. Fig. 12 shows the
 463 isolines of the joint probability density and failure probability at the nine representative nearshore
 464 stations. The most probable joint events with a 50-year and 100-year return period at the nine
 465 nearshore stations are then determined according to Fig. 12, as shown in Table 6.
 466



467

468 *Fig. 12 Isolines of the joint probability density and failure probability*

469

470 *Table 6 Most probable 50-year and 100-year return level joint events*

Station	50-year			100-year		
	Hs(m)	S(m)	CWL(m)	Hs(m)	S(m)	CWL(m)
Beihai	1.55	0.95	2.50	1.70	1.00	2.70
Dongfang	3.30	0.60	3.90	3.55	0.65	4.20
Haikou	4.25	0.95	5.20	4.65	1.35	6.00
Zhapo	5.25	1.65	6.90	5.65	1.85	7.50
Hong Kong	3.00	1.20	4.20	3.40	1.60	5.00
Xiamen	1.95	1.95	3.90	2.20	2.20	4.40
Kanmen	2.90	1.90	4.80	3.05	2.35	5.40
Lvsi	1.35	1.45	2.80	1.40	1.60	3.00
Shijiusuo	3.55	0.95	4.50	4.30	1.20	5.50

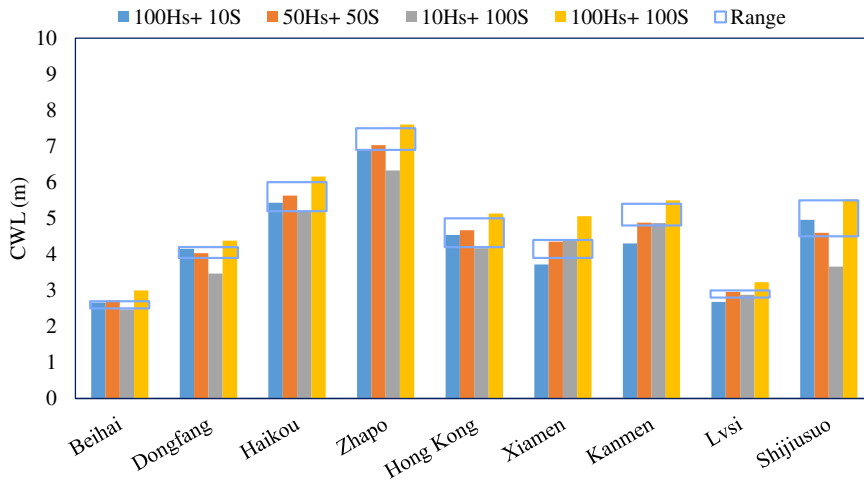
471

472 In engineering practice, when lacking the analysis of joint probability, the joint event for a certain
 473 period is typically estimated by an addition of the single event with specified return period. For
 474 example, a 100-year return level joint event is sometimes approximated by the sum of a 100-year

475 Hs (100Hs) and 10-year S (10S), the sum of a 10-year Hs (10Hs) and 100-year S (100S), or the sum
476 of a 50-year Hs (50Hs) and 50-year S (50S) (Li and Song, 2006), or an addition of 100-year Hs and
477 S (Code of Hydrology for Harhour and Waterway, JTS 145-2015, China). To compare the outcome
478 of these combinations and the joint probability results, the Hs and S sampled by the univariate
479 method without considering their dependence are used to calculate the Hs and S with 100-year,
480 50-year and 10-year return periods at all nine locations. The CWLs calculated by four empirical
481 combinations described above are compared with those calculated by the joint probability method
482 with the 50-year and 100-year return periods at the nine nearshore stations, as shown in Fig. 13,
483 where the ranges of the CWLs from the 50-year to 100-year return levels calculated by joint
484 probability method are presented for the sake of clarity. It can be seen from the figure that the
485 100-year CWLs calculated by joint probability method are larger than the “100Hs+10S,”
486 “50Hs+50S,” and “10Hs+100S” combinations but are smaller than the “100Hs+100S” combination.
487 In general, the “100Hs+10S” and “50Hs+50S” combinations are close to the 50-year return level
488 CWLs calculated by joint probability which could be recommended to estimate the 50-year return
489 level situation when the joint probability data is unavailable. Meanwhile, “50Hs+50S” combination
490 is always within the range of the 50-year and the 100-year return levels calculated by joint
491 probability method which could be a meaningful indicator for joint events between 50-year and
492 100-year return levels. The “10Hs+100S” combination is relatively smaller than other combinations,
493 especially at Beihai, Dongfang, Haikou, Zhapo, and Shijiusuo stations, which indicates a strong
494 wave predominant property.

495

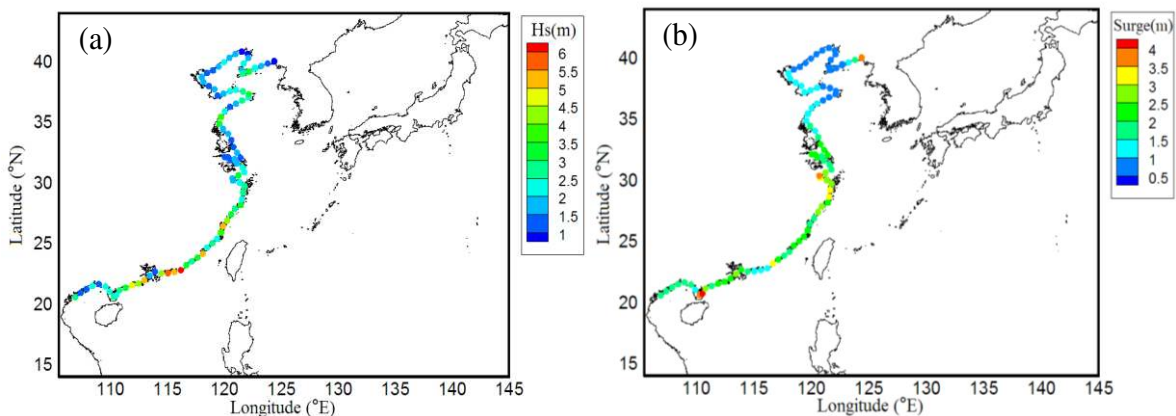
496 The result suggests that three of the empirical combinations may lead to an unsafe design, with only
497 the “100Hs+100S” combination being safe for an engineering design at all nine locations. However,
498 the method of using the “100Hs+100S” combination to estimate a 100-year joint event is proposed
499 based on the assumption that the Hs and S are independent random variables. This assumption may
500 be unrealistic because it has been proved that the Hs and S are partly dependent in this study, as
501 described in Section 4. Thus, it is necessary to conduct a joint probability analysis when designing
502 engineering structures.



503
 504 Fig. 13 The ranges of the CWL calculated by the joint probability method with GH copula for 50-year and
 505 100-year return periods (shown as a box) in comparison with the CWLs calculated by the empirical combinations
 506

507 **5. Discussion**

508 From the detailed comparison of the CWLs calculated by the empirical combination and joint
 509 probability method along the east coast of the mainland China, it is clear that the “100Hs+100S”
 510 combination is the only method which can lead to a safe design among the four empirical
 511 combinations. If this approach is adopted for the entire coastline, the extreme CWLs can be
 512 estimated for wide engineering applications. For the purposes of inter-comparison, Fig. 14 shows
 513 the distributions of the 100-year return level Hs and S at the studied coastline with 87 uniformly
 514 distributed locations. It can be seen from Fig. 14 (a) that the 100-year Hs along the southeast coast
 515 of the mainland China are remarkably larger than those at the other sites. However, in Fig. 14 (b),
 516 the distributions of the extreme S are rather uniform along the entire coast, with S being generally
 517 larger than 2 m from the mid-east to the south coast.



518
 519 Fig. 14 Distributions of the 100-year return level: (a) wave height and (b) surge level along the coasts of the
 520 mainland China without considering their dependence

521
522
523
524
525
526
527
528
529
530
531
532
533
534
535
536
537
538
539
540
541
542
543
544
545
546
547
548
549

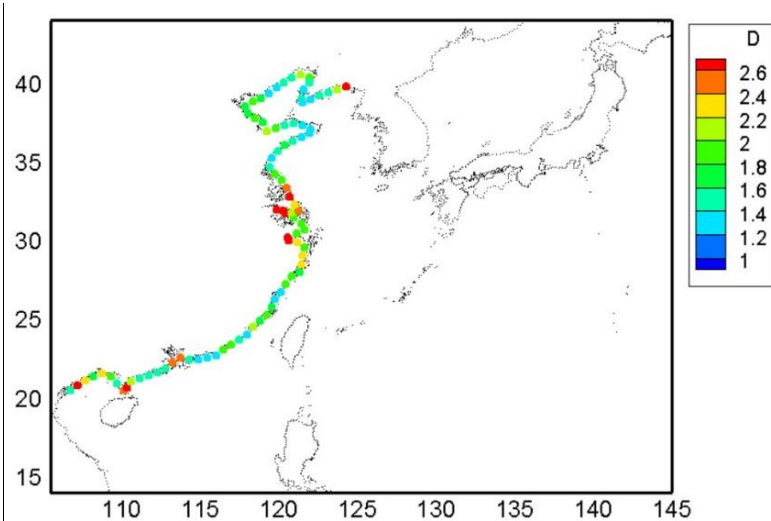
To investigate the hydrodynamic conditions for different areas in detail, a response coefficient (D) is defined as:

$$D = (H_s + S) / H_s \tag{14}$$

where H_s is the 100-year return level wave height and S is the 100-year return level surge.

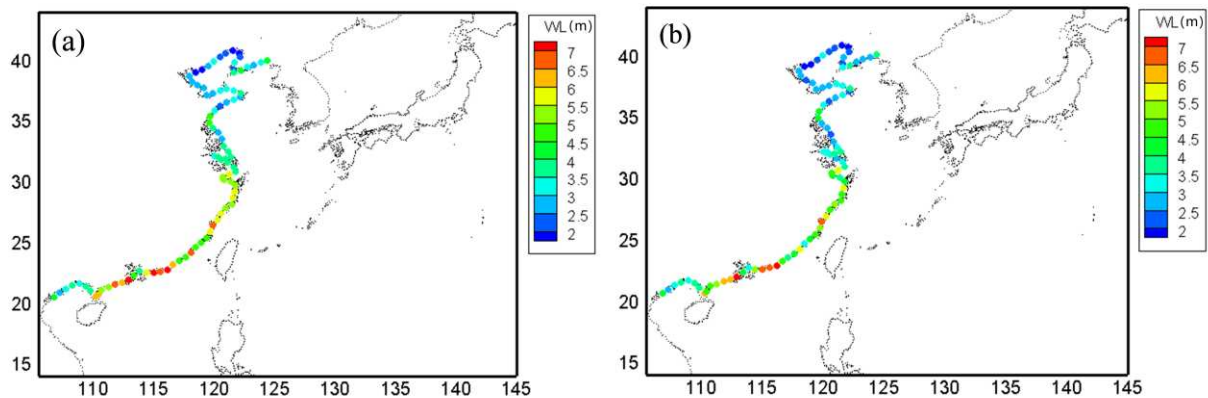
Although partly related, wave and surge are characterized by different dynamic, and have different magnitudes and spatial scales. As a coastal environment is usually defined as wave-predominated or surge-predominated based on the relative contributions of the wave and surge on coastal processes studied, as well as on coastal morphodynamics, the coefficient D could give a first impression on the relative significance of these two variables.

With the response coefficient (D) presenting the relative contributions of the H_s and S for the same return period at different locations, the hydrodynamic conditions there can then be described as wave-predominated or surge-predominated. D is generally larger than 1. If D is between 1 and 2, the location could be described as wave-predominated since the H_s has larger impact than S ; otherwise, if over 2, it is surge-predominated. The value of D could reflect the relative value of H_s and S . Higher values indicate a larger impact of S . Fig. 15 shows the distribution of coefficient D along the mainland China coast. It can be seen that coefficient D at most of the sites along the mainland China coast is between 1 and 2, which suggests that most of the areas along the mainland China coast are wave-predominated. The extreme wave height is obviously larger than surge level, which indicates a larger wave impact at these locations. This justifies the way that the joint extreme samples were selected in a wave-predominated manner in Section 3.1. For the southeast coast, the coefficient D is a little bit larger than 1, as these areas are facing open seas and are found in deep waters, which enhance the wave energy and mitigate the surge. However, in a few sites, D coefficients are far larger than 2, for example, the points in the Yangtze River estuary and Hangzhou bay. The water depths are small at these locations, and the shape of the estuary coastline may have caused surge to concentrate, resulting in those sites becoming surge-predominated.



550
551 *Fig. 15 Distribution of the response coefficient (D) along the coasts of the mainland China*
552

553 Furthermore, Fig. 16 shows the distributions of the 100-year return level CWLs, calculated by the
554 empirical method (100Hs+100S) and joint probability method. The distributions of the extreme
555 CWLs calculated by the joint probability method show a relatively higher value in the southeast
556 coast and lower value in the north. Although with the similar distribution patten, it is clear that using
557 the empirical method by assuming Hs and S being independent random variables can yield a higher
558 water level, but using the joint probability method can yield relatively more economical design
559 conditions.



560
561 *Fig. 16 Distribution of 100-year return level CWL calculated by the (a) empirical method (100Hs+100S) and (b)*
562 *joint probability method along the coasts of the mainland China*
563

564 As an indication of the improvement made between the 100-year CWLs calculated by the empirical
565 and joint probability methods, a parameter, Q, is introduced and defined as:

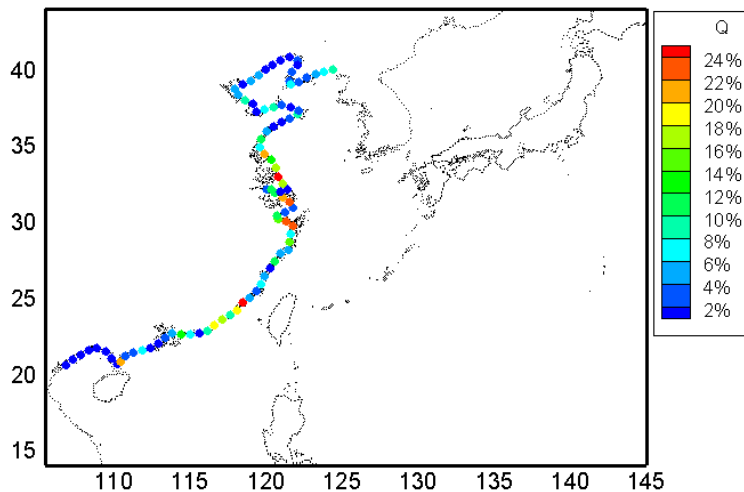
566
$$Q = \frac{CWL_e - CWL_j}{CWL_e} \times 100\% , \quad (15)$$

567 where, CWL_e is the water level calculated by the empirical method, and CWL_j is the water level
568 calculated by the joint probability method.

569

570 The distribution of the Q parameter shown in Fig. 17 indicates that the improvements in the joint
571 probability method compared with the empirical method are not notable in the north coast (Bohai
572 Sea coast) and south coast with a Q of under 6%, which means that the use of empirical
573 combinations at these locations is relatively reasonable. However, for the mid-east mainland coast
574 and southeast mainland coast, Q is relative larger, over 25% at its maximum. Thus, using the design
575 water level calculated by the empirical method at these locations may be inaccurate. In other words,
576 the joint probability method can yield better results at the sites where the hydrodynamic conditions
577 are generally complex or energetic. For example, two major estuaries (Yangtze and Hangzhou Bay)
578 are located the mid-east coast. The southeast coast is frequently affected by typhoon events,
579 particularly near the Taiwan Strait, which can incur stronger hydrodynamic processes and cause
580 larger diversity between water levels calculated by empirical and joint probability methods.

581



582
583 *Fig. 17 Distribution of the improvement coefficient along the mainland China coast*

584

585 6. Conclusions

586 This study uses long-term (35 years) model results to examine the suitability and performance of 4
587 copulas in the joint probability analysis of the extreme wave height (H_s) and surge (S) along the
588 coasts of the mainland China. The extreme data is extracted with the annual N-largest sampling

589 method and the dependencies between the Hs and S in the joint extreme samples at the nine selected
590 nearshore stations are fully analysed. The performance of the four commonly used copulas, i.e.
591 Gumbel-Hougaard, Clayton, Frank and Galambos copulas, in estimating the joint probability of
592 extreme samples are assessed. The optimal copula identified is used for predicting combined water
593 levels (CWLs, sum of Hs and S) in the study area with 50- and 100-year return periods and the
594 accuracy is quantified.

595

596 Two theoretical univariate probabilistic distributions, i.e. GEV and P3, are used to fit the marginal
597 of Hs and S samples. The results show that either GEV or P3 distributions could appropriately fit
598 the extreme wave samples which depends on their location, while the GEV distribution provides the
599 best fit to the extreme surge samples for all the selected locations along the mainland China coast.
600 After assessing the performance of the copulas, the extreme value copula group is found to be the
601 optimal copula group to describe the joint probability of extreme Hs and S. The Gumbel-Hougaard
602 copula that belongs to the extreme value copula group is finally chosen to conduct the joint
603 probability analysis of the Hs and S along the mainland China coast owing to its precision and
604 conciseness.

605

606 By adopting the GEV/P3 distribution and applying the copula theory, the joint exceedance
607 probabilities and joint probability densities at the nine representative nearshore stations are
608 calculated. The results at these locations show that there are no uniform distribution patterns of joint
609 distributions at different locations. The failure probability analysis is applied to calculate the most
610 probable CWLs. The analysis is also extended to the entire coastline of the study site at 87
611 uniformly distributed locations, where the coastline is clearly identified with the predominance of
612 the waves and surges. The empirical value of “100Hs+10S” and “50Hs+50S” combinations is
613 recommended to estimate the 50-year return level situation when the joint probability data is
614 unavailable and the “50Hs+50S” combination could be a meaningful indicator for events between
615 50-year and 100-year return levels. In comparison with the commonly used empirical design
616 approaches, the improvement coefficient (Q) is introduced and calculated, which suggests that
617 applying the joint probability approaches to the mid-east coast and southeast coast can improve the
618 accuracy in predicting extreme combined water levels with the given return period. The results from

619 this study provide reliable and realistic design guidelines for coastal engineering applications.

620

621 **Acknowledgements**

622 The work was partly supported by the National Key R&D Program of China (2017YFC0405401);
623 the National Natural Science Foundation of China (51909013, 51979076) and the Fundamental
624 Research Funds for the Central Universities, China (B200204017, 2019B04814)

625

626 **References**

- 627 Basco, D.R., Walker, R.A., 2010. Application of the Coastal Storm Impulse (COSI) parameter to
628 predict coastal erosion. In: Proceedings of the Coastal Engineering Conference.
- 629 Bernardara, P., Mazas, F., Kergadallan, X., Hamm, L., 2014. A two-step framework for
630 over-threshold modelling of environmental extremes. *Nat. Hazard. Earth Syst. Sci.* 14,
631 635-647. <https://doi.org/10.5194/nhess-14-635-2014>.
- 632 Bevacqua, E., Maraun, D., Vousdoukas, M. I., Voukouvalas, E., Vrac, M., Mentaschi, L., Widmann,
633 M., 2019. Higher probability of compound flooding from precipitation and storm surge in
634 Europe under anthropogenic climate change. *Sci. Adv.* 5. [https://doi.org/10.1126/sciadv.](https://doi.org/10.1126/sciadv.aaw5531)
635 aaw5531
- 636 Bruun, J.T., Tawn, J.A., 1998. Comparison of approaches for estimating the probability of coastal
637 flooding. *J. R. Stat. Soc.* 47, 405-423. <https://doi.org/10.1111/1467-9876.00118>.
- 638 Chebana, F., Ouarda, T.B.M.J., 2011. Multivariate quantiles in hydrological frequency analysis.
639 *Environ.* 22, 63-78. <https://doi.org/10.1002/env.1027>.
- 640 Chen, L., Singh, V.P., Guo, S., Hao, Z., Li, T., 2012. Flood coincidence risk analysis using
641 multivariate copula functions. *J. Hydrol. Eng.* 17, 742–755. [https://doi.org/10.1061/ \(ASCE\)](https://doi.org/10.1061/(ASCE)HE.1943-5584.0000504)
642 HE.1943-5584.0000504.
- 643 Chen, Y., Li, J., Pan, S., Gan, M., Pan, Y., Xie, D., Clee, S., 2019. Joint probability analysis of
644 extreme wave heights and surges along China's coasts. *Ocean. Eng.* 177, 97-107.
645 <https://doi.org/10.1016/j.oceaneng.2018.12.010>.
- 646 Chini, N., Stansby, P., Leake, J., Wolf, J., Roberts-Jones, J., Lowe, J., 2010. The impact of sea level
647 rise and climate change on inshore wave climate: A case study for East Anglia (UK). *Coast.*

648 Eng. 57, 973–984. <https://doi.org/10.1016/j.coastaleng.2010.05.009>.

649 Code of Hydrology for Harhour and Waterway (JTS 145-2015). China. 2015.

650 Coles, S., Heffernan, J., Tawn, J., 1999. Dependence measures for extreme value analyses. *Extrem.*
651 2, 339-365. <https://doi.org/10.1023/A:1009963131610>

652 Corbella, S., Stretch, D.D., 2012. Predicting coastal erosion trends using non-stationary statistics
653 and process-based models. *Coast. Eng.* 70, 40–49. [https://doi.org/10.1016/j.coastaleng.](https://doi.org/10.1016/j.coastaleng.2012.06.004)
654 2012.06.004.

655 Corbella, S., Stretch, D.D., 2013. Simulating a multivariate sea storm using Archimedean copulas.
656 *Coast. Eng.* 76, 68–78. <https://doi.org/10.1016/j.coastaleng.2013.01.011>.

657 De Michele, C., Salvadori, G., Vezzoli, R., Pecora, S., 2013. Multivariate assessment of droughts:
658 frequency analysis and dynamic return period. *Water Resour. Res.* 49, 6985–6994.
659 <https://doi.org/10.1002/wrcr.20551>.

660 De Waal, D.J., van Gelder, P.H.A.J.M., 2005. Modelling of extreme wave heights and periods
661 through copulas. *Extrem.* 8, 345–356. <https://doi.org/10.1007/s10687-006-0006-y>.

662 Dong, S., Jiao, C.S., Tao, S.S., 2017. Joint return probability analysis of wind speed and rainfall
663 intensity in typhoon-affected sea area. *Nat. Hazard.* 86, 1193-1205. [https://doi.org/10.1007/](https://doi.org/10.1007/s11069-016-2736-8)
664 [s11069-016-2736-8](https://doi.org/10.1007/s11069-016-2736-8).

665 Dong, S., Wang, N., Lu, H., Tang, L., 2015. Bivariate distributions of group height and length for
666 ocean waves using copula methods. *Coast. Eng.* 96, 49-61. [https://doi.org/10.1016/](https://doi.org/10.1016/j.coastaleng.2014.11.005)
667 [j.coastaleng.2014.11.005](https://doi.org/10.1016/j.coastaleng.2014.11.005).

668 Ferreira, J.A., Guedes Soares, C., 2002. Modelling bivariate distributions of significant wave height
669 and mean wave period. *Appl. Ocean Res.* 24, 31–45. [https://doi.org/10.1016/S0141-](https://doi.org/10.1016/S0141-1187(02)00006-8)
670 [1187\(02\)00006-8](https://doi.org/10.1016/S0141-1187(02)00006-8).

671 Fisher, N.I., Switzer, P., 2001. Graphical assessment of dependence: is a picture worth 100 tests?.
672 *Am. Stat.* 55, 233-239. <https://doi.org/10.1198/000313001317098248>.

673 Fisher, N. I., and Switzer, P., 1985. Chi-plots for assessing dependence. *Biom.* 72, 253-265.
674 <https://doi.org/10.2307/2336078>.

675 Galiatsatou, P., 2011. Bivariate analysis of extreme wave and storm surge events. determining the
676 failure area of structures. *Open Ocean Eng. J.* 4, 3-14. [https://doi.org/10.2174/1874835X](https://doi.org/10.2174/1874835X01104010003)
677 [01104010003](https://doi.org/10.2174/1874835X01104010003).

- 678 Galiatsatou, P., Prinos, P., 2007. Bivariate models for extremes of significant wave height and
679 period. An application to the Dutch Coast. In: Proceedings of 2nd IMA International
680 Conference on Flood Risk Assessment. University of Plymouth, UK.
- 681 Galiatsatou, P., Prinos, P., 2016. Joint probability analysis of extreme wave heights and storm surges
682 in the aegean sea in a changing climate. In: FLOODrisk 2016 - 3rd European Conference on
683 Flood Risk Management.
- 684 Genest, C., Favre, A.C., 2003. Everything You Always Wanted to Know about copula Modeling but
685 Were Afraid to Ask. Symmetries In Nuclear Structure: An Occasion to Celebrate the 60th
686 Birthday of Francesco Iachello.
- 687 Genest, C., Rivest, L.P., 1993. Statistical inference procedures for bivariate Archimedean copulas. *J.*
688 *Am. Stat. Assoc.* 88, 1034–1043. <https://doi.org/10.1080/01621459.1993.10476372>.
- 689 Gouldby, B., Méndez, F.J., Guanche, Y., Rueda, A. and Mínguez, R. 2014. A methodology for
690 deriving extreme nearshore sea conditions for structural design and flood risk analysis. *Coast.*
691 *Eng.* 88, 15-26. <https://doi.org/10.1016/j.coastaleng.2014.01.012>
- 692 Gruhn, A., Salecker, D., Fröhle, P., Schüttrumpf, H., Thorenz, F., 2012. Flood protection dunes – An
693 approach for reliability assessment by means of fragility curves as part of a risk and damage
694 analysis. In: Proceedings of 33rd International Conference on Coastal Engineering. Santander,
695 Spain.
- 696 Gudendorf, G., Segers, J., 2010. Extreme-value copulas, in: Jaworski, P., Durante, F., Härdle, W.K.,
697 Rychlik, T. (Eds.), *copula Theory and Its Applications*, Lecture Notes in Statistics. Springer,
698 Berlin Heidelberg.
- 699 Hawkes, P.J., Gouldby, B.P., Tawn, J.A., Owen, M.W., 2002. The joint probability of waves and
700 water levels in coastal engineering design. *J. Hydraul. Res.* 40, 241-251. [https://doi.org/10.](https://doi.org/10.1080/00221680209499940)
701 [1080/00221680209499940](https://doi.org/10.1080/00221680209499940).
- 702 Ji, X., Jing, D., Shen, H.W., Salas, J.D., 1984. Plotting positions for pearson type-III distribution. *J.*
703 *Hydrol.* 74, 1-29. [https://doi.org/10.1016/0022-1694\(84\)90137-9](https://doi.org/10.1016/0022-1694(84)90137-9).
- 704 Li, C., Song, Y., 2006. Correlation of extreme waves and water levels using a third-generation wave
705 model and a 3D flow model. *Ocean Eng.* 33, 635-653. [https://doi.org/10.1016/ j.oceaneng.](https://doi.org/10.1016/j.oceaneng.2005.06.003)
706 [2005.06.003](https://doi.org/10.1016/j.oceaneng.2005.06.003).
- 707 Li, F., van Gelder, P.H.A.J.M, Ranasinghe, R., Callaghan, D.P., Jongejan, R.B., 2014. Probabilistic

708 modelling of extreme storms along the dutch coast. *Coast. Eng.* 86, 1-13. <https://doi.org/10.1016/j.coastaleng.2013.12.009>.

709

710 Li, J., Pan, S., Chen, Y., Fan, Y., Pan, Y., 2018. Numerical estimation of extreme waves and surges
711 over the northwest Pacific Ocean. *Ocean. Eng.* 153, 225-241. [https://doi.org/10.1016/](https://doi.org/10.1016/j.oceaneng.2018.01.076)
712 [j.oceaneng.2018.01.076](https://doi.org/10.1016/j.oceaneng.2018.01.076).

713 Lin-Ye, J., Garcia-Leon, M., Gracia, V., Sanchez-Arcilla, A., 2016. A multivariate statistical model
714 of extreme events: an application to the Catalan coast. *Coast. Eng.* 117, 138-156. <https://doi.org/10.1016/j.coastaleng.2016.08.002>.

715

716 Martzikos, N.T., Prinos, P.E., Memos, C.D., Tsoukala, V.K., 2021. Key research issues of coastal
717 storm analysis. *Ocean. Coast. Manag.* 199, 105389. [https://doi.org/10.1016/](https://doi.org/10.1016/j.ocecoaman.2020.105389)
718 [j.ocecoaman.2020.](https://doi.org/10.1016/j.ocecoaman.2020.105389)
[105389](https://doi.org/10.1016/j.ocecoaman.2020.105389)

719 Marcos, M., Rohmer, J., Vousdoukas, M. I., Mentaschi, L., Le Cozannet, G., Amores, A., 2019.
720 Increased extreme coastal water levels due to the combined action of storm surges and wind
721 waves. *Geophys. Res. Lett.* 46, 4356-4364. <https://doi.org/10.1029/2019GL082599>

722 Masina, M., Lamberti, A., Archetti, R., 2015. Coastal flooding: a copula based approach for
723 estimating the joint probability of water levels and waves. *Coast. Eng.* 97, 37-52.
724 <https://doi.org/10.1016/j.coastaleng.2014.12.010>.

725 Mazas, F., Hamm, L., 2017. An event-based approach for extreme joint probabilities of waves and
726 sea levels. *Coast. Eng.* 122, 44-59. <https://doi.org/10.1016/j.coastaleng.2017.02.003>.

727 Mazas, F., Kergadallan, X., Garat, P., Hamm, L., 2014. Applying POT methods to the revised joint
728 probability method for determining extreme sea levels. *Coast. Eng.* 91, 140-150. <https://doi.org/10.1016/j.coastaleng.2014.05.006>.

729

730 Mikosch, T., 2006. Copulas: Tales and facts. *Extrem.* 9, 3–20. [https://doi.org/10.1007/s10687-006](https://doi.org/10.1007/s10687-006-0015-x)
731 [-0015-x](https://doi.org/10.1007/s10687-006-0015-x).

732 Montes-Iturrizaga, R., Heredia-Zavoni, E., 2015. Environmental contours using copulas. *Appl.*
733 *Ocean. Res.* 52, 125-139. <https://doi.org/10.1016/j.apor.2015.05.007>.

734 Montes-Iturrizaga, R., Heredia-Zavoni, E., 2016, Multivariate environmental contours using c-vine
735 copulas. *Ocean. Eng.* 118, 68-82. <https://doi.org/10.1016/j.oceaneng.2016.03.011>.

736 Pearson, K., 1895. Mathematical contributions to the theory of evolution. iii. regression, heredity,
737 and panmixia. *Philosophical Transactions of the Royal Society of London A*, 186(4), 343-414.

738 <https://doi.org/10.1098/rsta.1895.0010>

739 Qi, J., Chen, C., Beardsley, R.C., Perrie, W., Cowles, G.W., Lai, Z., 2009. An unstructured grid
740 finite-volume surface wave model (FVCOM-SWAVE): implementation, validations and
741 applications. *Ocean Model.* 28, 153–166. <https://doi.org/10.1016/j.ocemod.2009.01.007>

742 Rueda, A., Camus, P., Tomás, A., Vitousek, S., Méndez, F. J., 2016. A multivariate extreme wave
743 and storm surge climate emulator based on weather patterns. *Ocean. Model.* 104, 242-251.
744 <https://doi.org/10.1016/j.ocemod.2016.06.008>.

745 Serafin, K.A. and Ruggiero, P., 2014. Simulating extreme total water levels using a time-dependent
746 extreme value approach. *J. Geophys. Res. Ocean.* 119, 6305-6329. [https://doi.org/](https://doi.org/10.1002/2014jc010093)
747 [10.1002/2014jc010093](https://doi.org/10.1002/2014jc010093)

748 Salvadori, G., De Michele, C., 2004. Frequency analysis via copulas: Theoretical aspects and
749 applications to hydrological events. *Water Resour. Res.* 40, W12511. [https://doi.org/](https://doi.org/10.1029/2004WR003133)
750 [10.1029/2004WR003133](https://doi.org/10.1029/2004WR003133).

751 Salvadori, G., Durante, F., Tomasicchio, G.R., D'Alessandro, F., 2015. Practical guidelines for the
752 multivariate assessment of the structural risk in coastal and off-shore engineering. *Coast. Eng.*
753 95, 77-83. <https://doi.org/10.1016/j.coastaleng.2014.09.007>.

754 Sklar A., 1959. Fonctions de répartition à n dimensions et leurs marges. *Publ. Inst. Statist. Univ.*
755 *Paris.* 8, 229-231.

756 Sraj, M., Bezak, N., Brilly, M., 2015. Bivariate flood frequency analysis using the copula function:
757 a case study of the litija station on the sava river. *Hydrol. Processes.* 29, 225-238.
758 <https://doi.org/10.1002/hyp.10145>.

759 Tao, S., Dong, S., Wang, N., Soares, C.G., 2013. Estimating storm surge intensity with Poisson
760 bivariate maximum entropy distributions based on copulas. *Nat. Hazard.* 68, 791-807.
761 <https://doi.org/10.1007/s11069-013-0654-6>.

762 Tawn, J.A., 1998. An extreme-value theory model for dependent observations. *J. Hydrol.* 10,
763 227-250. [https://doi.org/10.1016/0022-1694\(88\)90037-6](https://doi.org/10.1016/0022-1694(88)90037-6).

764 Vanem, Erik, 2016. Joint statistical models for significant wave height and wave period in a
765 changing climate. *Mar. Struct.* 49, 180-205. <https://doi.org/10.1016/j.marstruc.2016.06.001>.

766 Wahl, T., Plant, N. G., Long, J.W., 2016. Probabilistic assessment of erosion and flooding risk in the
767 northern gulf of mexico. *J. Geophys. Res. Ocean.* 121, 3029-3043. <https://doi.org/10.1002/2016JC012000>

768 org/10.1002/2015JC011482.

769 Wahl, T., Jensen, J., Mudersbach, C., 2010. A multivariate statistical model for advanced storm
770 surge analyses in the North Sea. In: 32rd International Conference on Coastal Engineering.
771 Shanghai, China.

772 Wahl, T., Mudersbach, C., Jensen, J., 2012. Assessing the hydrodynamic boundary conditions for
773 risk analyses in coastal areas: a multivariate statistical approach based on copula functions. *Nat.*
774 *Hazard. Earth Syst. Sci.* 12, 495–510. <https://doi.org/10.5194/nhess-11-2925-2011>.

775 Ward, P. J., Couasnon, A., Eilander, D., Haigh, I.D., Hendry, A., Muis, S., Veldkamp, T.I.E.,
776 Winsemius, H.C., and Wahl, T., 2018. Dependence between high sea-level and high river
777 discharge increases flood hazard in global deltas and estuaries. *Environ. Res. Lett.* 13, 084012
778 <https://doi.org/10.1088/1748-9326/aad400>

779 Wist, H.T., Myrhaug, D., 2004. Statistical properties of successive wave heights and successive
780 wave periods. *Appl. Ocean. Res.* 26, 114–136. <https://doi.org/10.1115/1.2829561>.

781 Yang, X., Qian, J., 2019. Joint occurrence probability analysis of typhoon-induced storm surges and
782 rainstorms using trivariate Archimedean copulas. *Coast. Eng.* 171, 533-539. <https://doi.org/10.1016/j.oceaneng.2018.11.039>.

784 Yang, X.C., Zhang, Q.H., 2013. Joint probability distribution of winds and waves from wave
785 simulation of 20 years (1989-2008) in bohai bay. *Water. Sci. Eng.* 6, 296-307.
786 <https://doi.org/10.3882/j.issn.1674-2370.2013.03.006>.

787 Yin, K., Xu, S., Huang, W., 2018. Estimating extreme sea levels in Yangtze Estuary by quadrature
788 Joint Probability Optimal Sampling Method. *Coast. Eng.* 140, 331-341. <https://doi.org/10.1016/j.coastaleng.2018.08.007>.

790 Zhang, L., Singh, V.P., 2007. Bivariate rainfall frequency distributions using Archimedean copulas.
791 *J. Hydrol.* 332, 93–109. <https://doi.org/10.1016/j.jhydrol.2006.06.033>.

792 Zhang, Y., Kim, C.W., Beer, M., Dai, H., Soares, C.G., 2018. Modeling multivariate ocean data
793 using asymmetric copulas. *Coast. Eng.* 135, 91-111. <https://doi.org/10.1016/j.coastaleng.2018.01.008>.

794 2018.01.008.